Journal of Applied Electrochemistry (2007) 37:87–93
DOI 10.1007/s10800-006-9206-z

Computer aided fuel cell design and scale-up, comparison between model and experimental results

G. SQUADRITO, O. BARBERA*, G. GIACOPPO, F. URBANI and E. PASSALACQUA
CNR-ITAE, Via Salita S. Lucia sopra Contesse 5, 98126, Messina, Italy
*(*author for correspondence, e-mail: orazio.barbera@itae.cnr.it)*

Received 14 February 2006; accepted in revised form 6 June 2006

Key words: CFD, design correlation, flow field design, PEM fuel cell, serpentine channels

Abstract

The present work illustrates the employment of an Automatic Scale-up Algorithm (ASA) to design a 200 cm^2 multiple serpentine (MS) flow field for a Polymer Electrolyte Fuel Cell (PEFC). With a fixed fuel cell active area and total pressure drop, the algorithm provides the flow-field design solution characterized by a specific set of parameters including channel width, rib width, channel height, covering factor, number of switchbacks, Reynolds number and pressure drop. It is known that a correlation exists between the mass flow passing through the electrode and the pressure drop, influencing the fuel cell performance. A pressure drop range from 5 to 45 kPa with steps of 5 kPa has been investigated. Numerical simulations performed on each geometry set have permitted a comparison of the flow-field total pressure drop with the analytical compressible calculation, and to evaluate the mass flow rate passing through the electrode and in the flow field channels separately. A comparison between ASA and CFD results has highlighted that the methodology is able to find a flow-field geometry that matches target geometrical and fluid dynamic requirements. A better agreement between the Automatic Scale-up Algorithm and direct CFD pressure drop calculation has been obtained taking into account the gas compressibility effects. The increase of the mass flow rate vs flow-field total pressure drop is also reported. A better understanding of the gas shorting phenomenon has been achieved by CFD post-processing, in terms of gas velocity profiles and pressure drop between adjacent channels. Since the gas shorting is a pressure driven effect, the total mass flow rate percentage passing through the porous backing has been related to the shorting velocity and geometrical parameters of the porous backing; moreover proportionality between "shorting" pressure drop and ratio of flow field total pressure drop and switchback number has been highlighted.

1. Introduction

The interaction between the flow field and the electrode diffusion layer plays a primary role in the performance of PEFCs [1–3]. Soon et al. [4] proposed a novel configuration of partially blocked fuel channels to enhance reactant gas transport from channels to diffusion layer regions and Maharudrayya et al. [5] introduced new correlations to calculate pressure losses in the flow distributor plate for laminar flows. Nevertheless, no guidelines or project methodology that are based on precise specifications such as the electrode active area, MEA aspect ratio, channel pressure losses and Reynolds number have been provided for designers of fuel cell flow fields. Taking advantage of the reliability of Computational Fluid Dynamic (CFD) simulations, a computer aided fuel-cell design methodology that regards a serpentine like flow field (single serpentine, ribbed serpentine and multiple serpentine) has been realised [6]. It includes an automatic algorithm for flow-field generation and selection. The automatic algorithm for flow-field generation produces the parameters of all of the possible serpentines that can cover a fixed active area. Among the obtained solutions the automatic algorithm of flow-field selection provides a set of flow-field, matching the target variables fixed by the user. The consistency of the proposed procedure is under investigation. In [6] this methodology was applied to scale up to 50 cm^2–5 cm^2 PEFC having a ribbed serpentine flow field. Two solutions characterized by a different flow rate ratio between the gas in the diffusion layer and in the channels (ψ) were evolved and tested. Despite a geometrical similarity between the compared flow-fields, the fluid dynamic behaviour and the I–V experimental curves were found to be different especially at high current density. The worst performance in the diffusive region was given by the flow-field having a lower ψ value. In fact, at high current densities a higher flow velocity through the electrode backing would be appropriate to avoid starvation problems and remove the considerable amount of water produced. The present work describes a further application of the methodology

to design the plates for a 1 kW PEM fuel cell stack with a 200 cm^2 active area in a slim configuration and $\zeta = 1/3$ (shape factor, active area width/height). Selected flow fields have been analysed by a commercial CFD solver (Star-CD® release 3.24) to evaluate the mass flow passing through the electrode which depends on flow field geometric parameters. A comparison between the calculated flow field total pressure drop and those obtained by numerical simulation was also carried out. Post-processing analysis has permitted new interesting results regarding the flow field and electrode backing interaction to be obtained. In particular a direct dependence of the gas shorting phenomenon on the flow field geometry was highlighted.

2. Experimental methods

2.1. *Flow field set generation*

A 50 cm^2 cell was chosen as a reference and operative conditions regarding flow-field typology and I–V curves were fixed as an input for the Automatic Scale-up Algorithm (ASA) [6]. In this case, the active area (AMEA) of 200 cm^2 and a flow field shape factor (ζ = width/height) of 1/3 were set and a pressure drop (Δp) ranging from 5 to 45 kPa was investigated. The ASA was used to find the geometric flow field parameters matching the requested pressure drop by varying the input variables in the ranges shown in Table 1.

Figure 1 shows the software flow-chart where input and output variables coming in from/out of each subroutine are highlighted. The main routine spans the pressure drop (Δp_i) from a minimum to a maximum value with a defined increase. For each Δp_i the routine calculates the variables to send to Flow field Generation Software (FGS), which takes into account these parameters and generates the whole set of solutions which respect the variation range of geometrical parameters. At this stage, the Flow-path Generation Parameters (FGPs), Design Coefficients (DCs) and Fluid Dynamic Quantities (FDQ) are also determined. The flow field selection is made by the Selection Algorithm Software (SAS) that filters the FGS output and provides the solution on the basis of the following constrains:

$$\zeta_i = \pm 5\%\, \zeta_{\text{fixed}}, \quad \Delta p_i = \pm 5\%\, \Delta p_{\text{mi}}. \tag{1}$$

Table 1. ASA input variables and ranges

Parameter name	Parameter meaning	Range
LCOS/mm	Rib width	$0.50 \div 1.0$
HCAN/mm	Channel height	$0.5 \div 1.0$
LCAN/mm	Channel width	$0.5 \div 2.5$
A_{in}/mm^2	Inlet area	< 10
ζ	Shape factor	1/3
χ	Covering factor	$50\% \div 65\%$

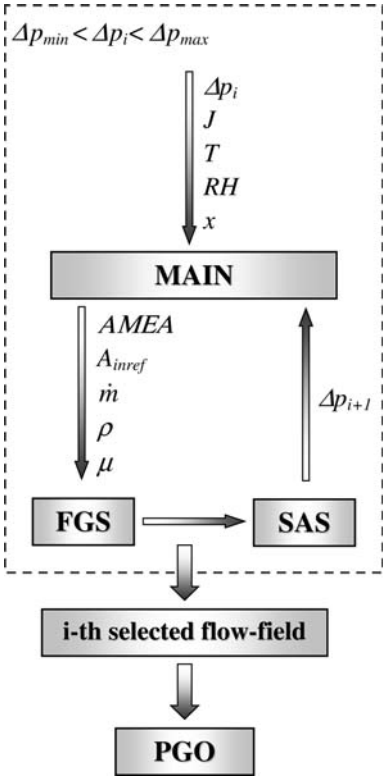

Fig. 1. ASA flow-chart.

Subscript "*i*" for the pressure drop (Δp) indicates the *i*th Δp_{m} value that has to be matched by ASA and the value calculated according to the constraints, respectively. The calculated Δp is related to the flow field parameters by a suitable relation:

$$\Delta p = f(\text{FGPs}). \tag{2}$$

2.2. *CFD model assumptions*

The steady state numerical model was assumed in isothermal, single component and single phase conditions, in fact the gas was treated as perfect mixture of air and water vapour whose thermodynamic and physical properties (gas constant, density, viscosity specific heat etc.) were calculated by averaging the single component properties. The gas flow was considered to be compressible; thus its density is determined by the perfect gas law. On the basis of the operating conditions, Navier–Stokes equations were solved in the laminar form. Electrochemical aspects were not considered because the principle aim of the work is to provide a simple flow-field design method based on knowledge of the mechanical and fluid dynamic parameters of the reference cell. The flow-field/electrode system was modelled as a fluid region constituted by a flow-path on which a porous layer was superimposed. The porous electrode was considered as an isotropic medium that acts as a momentum sink for the gas flowing into it. The basic transport equations (conservation of mass and momentum) were written for each zone of the domain.

Table 2. Physical parameters used in the CFD calculation

$T_{in} = 353$	Mixture inlet temperature/K
$p_{out} = 1.5 \times 10^5$	Mixture pressure at outlet/Pa
$\rho_{in} = 1.325$	Inlet mixture density/kg m^{-3}
$\mu = 3.32 \times 10^{-5}$	Mixture molecular viscosity/Pa s^{-1}
$\dot{m} = 9.58 \times 10^{-5}$	Mass flow rate/kg s^{-1}

A source term (properly a sink) was introduced in the momentum equations, for the porous layer only.

2.3. *Boundary conditions*

Boundary conditions were applied at the inlet and outlet cross-section of the model. A constant mass flow rate was imposed as an inlet boundary, whereas a constant pressure was applied at the outlet region. These boundaries are the most similar to real fuel cell operation. In fact, fuel cell test stations generally impose a constant mass flow rate at the inlet by a mass flow controller and a fixed outlet pressure by a backpressure valve. The adopted operative conditions are summarized in Table 2.

2.4. *Solution strategy*

The model equations were solved by the control volume technique; thus the domain was divided into hexahedron volume elements leading to a maximum total number of computational cells of about one million. The adopted grid was of a structured type and mesh refinements were utilised in the sharp bends especially, where a large velocity variation is expected. The porous media was modelled assuming that within the volume containing the distributed resistance, a local balance between pressure and resistance forces exists, such as:

$$\frac{\partial p}{\partial x_i} = -K_i v_{spi} \tag{3}$$

where x_i (i = 1,2,3) represents the (mutually orthogonal) orthotropic directions, K_i is the permeability, v_{spi} is the superficial velocity in direction x_i. The permeability K_i is assumed to be a quasi-linear function of the superficial velocity magnitude in the form:

$$K_i = \alpha_i \left|\vec{v}_{sp}\right| + \beta_i \tag{4}$$

where α_i and β_i are user supplied coefficients, which may be either uniform or spatially varying. In this work a constant value of α_i and β_i was chosen on the basis of literature data [3], in particular

$$\alpha_i = 0/\text{kg m}^{-4}; \quad \beta_i = 2 \times 10^7/\text{kg m}^3\text{s}. \tag{5}$$

The solution strategy is based on the SIMPLE algorithm [7]. Step by step, the velocity computed from the linearised momentum equation and an estimate of the pressure field were taken as provisional values used to solve the continuity equation. Once the continuity equation terms were balanced, the pressure correction value was used to update the pressure and velocity values.

3. Results and discussion

3.1. *Pressure drop flow-field study*

The explicit form of the aforementioned Equation (2) is the following:

$$\begin{aligned} \Delta p_{inc} &= -\lambda Re^2 \frac{\mu^2}{2\rho D_h^3} \cdot \xi \\ &= -\lambda \frac{\dot{m}^2}{4\rho} \cdot \frac{\text{LCAN} + \text{HCAN}}{(\text{LCAN} \cdot \text{HCAN})^3 \cdot \text{NDIV}^2} \cdot \xi \end{aligned} \tag{6}$$

where Re is the Reynolds number, μ the fluid viscosity ρ the fluid density, D_h the hydraulic diameter, λ the friction factor, $\dot{m}$ the gas flow rate and ξ is the serpentine length that is equivalent to the gas flow path mean line length:

$$\xi = \frac{A_{lib}}{\text{NDIV} \cdot \text{LCAN}} \tag{7}$$

where A_{lib} represents the top surface area of the channels, NDIV the parallel serpentine number.

The bend loss component was neglected because Re never exceeds 550, so that the main contribution to pressure losses is due to the pipe frictional resistances [5]. Moreover, the adopted flow field design methodology keeps the stream tube cross-sectional area fixed along the entire flow field that avoids a further stream contraction or expansion losses.

As Table 3 and Figure 2 report, a good agreement between Δp_{inc} (Equation 6) and Δp_m was achieved, this reveals the ability of ASA to find the right geometrical

Table 3. Flow field parameters selected by ASA (incompressible)

Δp_m/kPa	FGPs					DCs			FDQ		
	LCOS/mm	LCAN/mm	HCAN/mm	N	NDIV	A_{in}/mm^2	ζ	χ	Δp_{inc}/kPa	v_{in}/m s^{-1}	Re
5	1.0	1.6	1.0	5	6	9.60	0.30	0.63	6.88	7.53	369.98
10	0.9	1.1	1.0	5	8	8.80	0.31	0.56	10.08	8.21	343.55
15	1.0	1.0	0.9	5	8	8.00	0.31	0.51	15.09	10.04	379.72
20	1.0	1.2	1.0	7	5	6.00	0.29	0.55	19.88	12.05	524.70
25	1.0	1.2	0.9	7	5	6.00	0.29	0.55	24.85	13.39	549.69
30	0.8	1.1	0.8	7	6	6.60	0.31	0.59	30.12	13.69	506.29
35	0.7	1.2	0.7	7	6	6.60	0.31	0.64	34.58	14.34	506.29
40	0.8	1.1	0.7	7	6	6.60	0.31	0.59	40.36	15.65	534.42
45	0.7	0.7	0.9	7	8	5.60	0.30	0.51	44.38	14.34	450.91

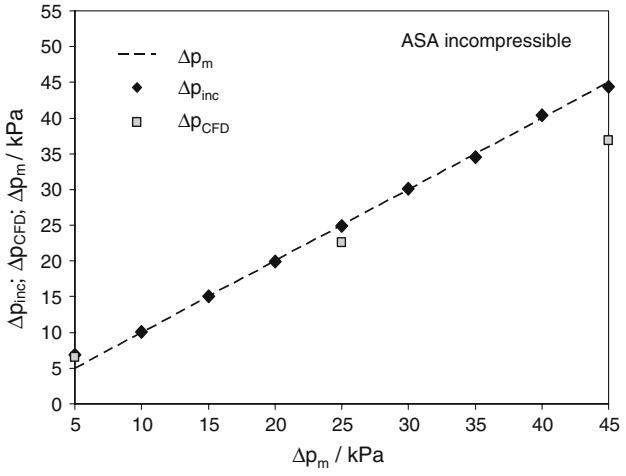

Fig. 2. Δp comparison: ASA incompressible formulation vs CFD.

parameters that respect the requested flow field overall pressure drop in accordance with the structural constrains listed in Table 1. A check of ASA solution reliability was made by comparing the total pressure drop calculated by correlation with those obtained by numerical fluid dynamic analysis (CFD).

Results show that this method gives a good agreement in the range from 5 to 25 kPa where the percentage error is below 10%. By increasing the total pressure drop, Equation (6) overvalues the CFD results with a maximum percentage error of 20% at 45 kPa and this error seems to grow with a linear trend.

A better agreement has been achieved by introducing the density variation along the flow path that modifies Equation (6) as follows:

$$p_{\text{out}}^2 - p_{\text{in}}^2 = -\lambda Re^2 \frac{\mu^2 \mathscr{R} T}{2\mathscr{M} D_{\text{h}}^3} \cdot \xi = -\lambda \frac{\dot{m}^2 \mathscr{R} T}{4\mathscr{M}} \frac{\text{LCAN} + \text{HCAN}}{(\text{LCAN} \cdot \text{HCAN})^3 \cdot \text{NDIV}^2} \cdot \xi \quad (8)$$

where $\mathscr{R}$ is the universal gas constant and $\mathscr{M}$ the reactant molecular weight. In Equation (8), density is a function of pressure and temperature T that, coherently with the model assumption, is considered as a constant (§ 2.1). Equation (8) implies an implicit formulation of pressure drop; thus Δp_{comp} is computable only if the inlet pressure (p_{in}) or outlet pressures (p_{out}) are known. Table 4 shows the flow field parameters obtained using correlation (8).

Despite the same structural constrains, the ASA compressible solution (Table 4) differs from that obtained by incompressible correlation in terms of FGPs; however the DCs tolerance is maintained in the assigned range. Figure 3 shows a better agreement between the CFD and ASA compressible pressure drop calculation, indeed in the overall pressure drop range, the percentage error stands in a band which never exceeds 7% (Figure 3). It seems logical to conclude that the density variation along the flow path becomes relevant when the serpentine flow field pressure drop goes beyond 25 kPa. Therefore, in a typical fuel cell application, where a total pressure drop of about 10–20 kPa is suitable, an incompressible formulation could be used with sufficient reliability.

3.2. *Pressure drop Flow-field and porous layer study*

The presence of a convective secondary flow of the fluid in the porous layer in addition to the main flow in the channels has been highlighted [3]. This phenomenon, known as ''gas shorting'' [8], has to be considered in a flow field design because it can negatively or positively influence the fuel cell performance. It could be negative when the reactant bypasses regions of the active area flow under the landing rather than along the channel flow path. This can occur in the serpentine flow path, especially in the switchbacks, because of the differential pressure between adjacent channels and momentum variation close to the corners. The cell performance can be enhanced by gas shorting when reactants are forced into the gas diffusion region, this permits liquid water to be driven out of the electrode. Figure 4(a) shows velocity profiles along a flow field plus porous layer cross-section, and how the CFD is able to display the above cited phenomenon. In Figure 4(b) the total pressure drop of a selected flow field having a Δp_{m} of 10 kPa (Table 3) is also reported, where the amplitude of discontinuities represents a Δp_{sh} of about 1.1 kPa. Numerical simulation has also permitted an evaluation the portion of total mass flow rate (ψ) that passes through the electrode backing as a quantification of the

Table 4. Flow field parameters selected by ASA (compressible)

Δ_{m}/kPa	FGPs					DCs			FDQ		
	LCOS/mm	LCAN/mm	HCAN/mm	N	NDIV	A_{in}/mm^2	ζ	χ	Δp_{comp}/kPa	v_{in}/m s^{-1}	Re
5	1.0	1.6	1.0	5	6	9.60	0.30	0.63	6.73	7.53	370.06
10	1.0	1.2	1.0	5	7	8.40	0.29	0.55	9.82	8.61	374.86
15	1.0	1.6	0.7	5	6	9.60	0.30	0.63	14.96	10.76	418.33
20	0.5	0.9	1.0	7	8	7.20	0.30	0.65	20.08	10.04	379.80
25	0.6	0.8	1.0	7	8	6.40	0.30	0.58	25.29	11.30	400.90
30	0.8	1.4	0.7	7	5	7.00	0.29	0.64	30.16	14.76	549.80
35	1.0	1.2	0.9	9	4	4.80	0.31	0.55	34.83	16.74	687.25
40	0.7	1.0	0.9	9	5	5.00	0.29	0.60	40.01	16.07	607.67
45	0.8	1.4	0.7	9	4	5.60	0.31	0.64	45.10	18.45	687.25

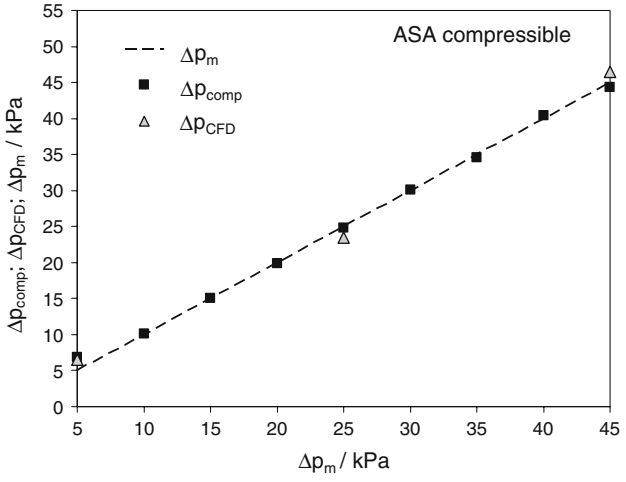

Fig. 3. Δp comparison: ASA compressible formulation vs CFD.

gas shorting phenomenon. This was defined as follows:

$$\psi = \frac{\dot{m}_{sp}}{\dot{m}} \cdot 100 \tag{9}$$

where $\dot{m}_{sp}$ represents the mass passing through the electrode and $\dot{m}$ the total mass flow rate. This information was carried out on the basis of the obtained velocity profiles in the fuel cell cross-section provided by numerical simulations (Figure 4).

The velocity average value $\bar{v}_{sp}$ was obtained by averaging numerical velocity profiles on a longitudinal section of the porous layer and it was successively used to calculate $\dot{m}_{sp}$ according to the following correlation:

$$\dot{m}_{sp} = \rho \cdot \mathrm{HMEA} \cdot s \cdot \bar{v}_{sp} \tag{10}$$

where ρ is the mean gas density at the fixed section area, HMEA is the MEA height and s is the porous layer thickness. In Figure 5 the dependance of ψ on Δp_m is shown at fixed operating conditions (Table 2). As can be seen, the mass flow rate crossing the porous layer increases with total pressure drop.

Despite the performance enhancement related to a greater ψ significant increase in pressure drop is needed; this implies a greater energy to supply reactants to the cell. However, by analysing the ASA output it was noted that ψ depends on both the total pressure drop and the geometrical parameters. Table 5 reports ψ values obtained by CFD analysis for two serpentine flow fields with a similar pressure drop but different design parameters.

Table 5 shows that the solution with a higher ψ is characterized by a lower switchback number (N). In fact, considering fixed electrode porosity, similarity between Δp_{inc} of selected flow fields, and observing that the amplitude of discontinuities in Figure 4(b) is constant, it is evident that Δp_{sh} is proportional to $\Delta p_{inc}/N$. Therefore a lower N implies a Δp_{sh} increase followed by a greater $\bar{v}_{sp}$ (Equation 3), thus resulting in an increase in mass flow rate passing through the electrode backing (Equation 10).

3.3. *Application*

The proposed methodology could be useful for the fuel cell designer due to its flexibility. In fact ASA has been applied to design a 200 cm^2 bipolar plate for a 1 kW fuel cell stack in a slim configuration. Moreover, as Figure 6 depicts, ASA could be easily interfaced with a CFD/FEM software analysis to predict the fluid dynamic and structural behaviour of a designed plate and a CAD/CAE applications for rapid prototyping and manufacturing. It is also a useful tool for investigation since the entire set of FF parameters could be related to experimental results.

The driving idea in the FF choice was to have the same ψ value of the reference cell. Consequently the FF

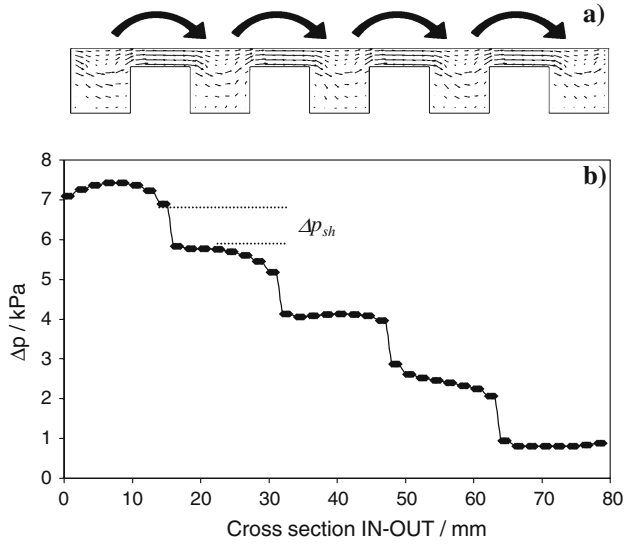

Fig. 4. Velocity profile (a) and pressure drop (b) along a flow field plus porous layer cross-section.

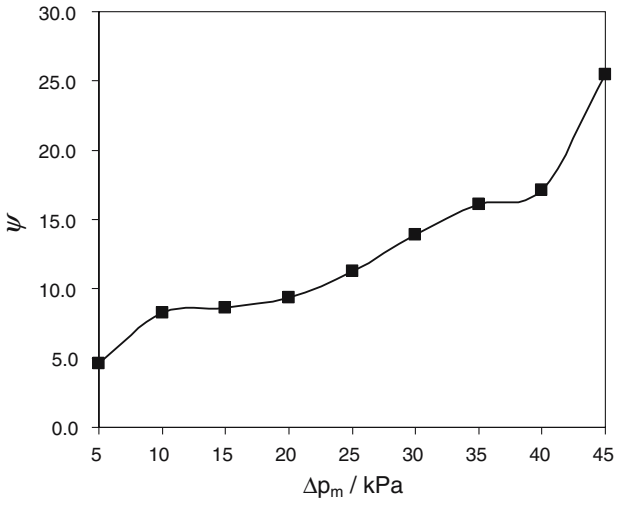

Fig. 5. ψ behaviour at various Δp_m.

Table 5. Comparison between two ASA solutions having similar Δp_{inc}

Δp_m/kPa	Δp_{in}/kPa	ψ	Δp_{CFD}/kPa	N
45	44.68	15.55	39.20	11
45	44.37	25.47	36.80	7

an excessive flow field overall pressure drop is detrimental in terms of plant efficiency because of a dramatic increase in parasitic losses due to the compressor. The methodology developed is able to fulfil both highlighted aspects, since it allows all the flow field geometrical parameters to be identified *a priori* and the most important fluid dynamic quantities related to it to be evaluated. In this work a computer aided FF design and a characterization (ASA) were applied to a 200 cm^2 active area flow field and tested to understand how the ψ parameter is related to the FF overall pressure drop and find a correct geometrical parameter set that allows scale-up of the reference cell. Two sets of flow fields with a pressure drop in the range 5–45 kPa were generated, one using an incompressible pressure drop formulation, the other a compressible one. A comparison between CFD results and ASA output has shown that compressibility effects become relevant for a Δp greater than 25 kPa. Direct numerical simulations performed on a "FF + porous layer" system have shown that ψ is strictly related to the shorting phenomenon, that, in turn, is affected by the overall pressure drop and switchback number N.

The results are encouraging enough to proceed with the investigation that will in future provide a guideline

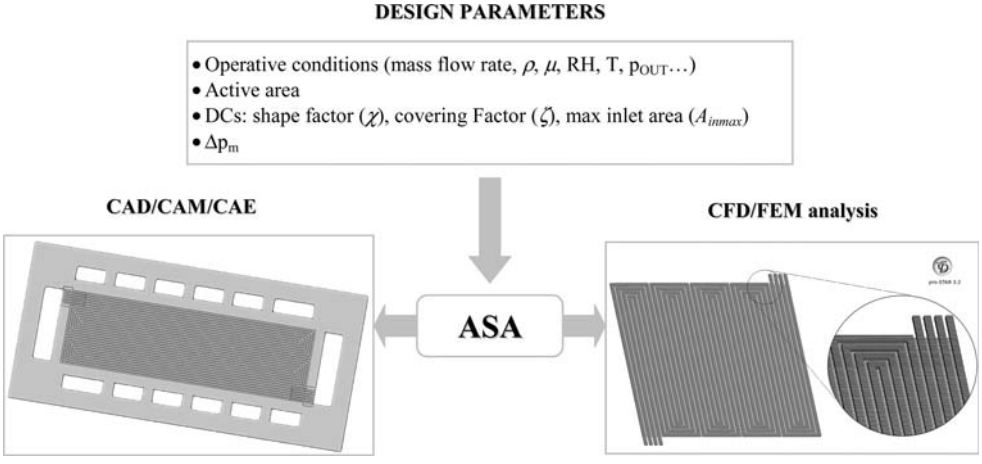

Fig. 6. Schematic representation of ASA purposes.

that matches this constraint is formed by six parallel serpentines with a Δp_m of 5 kPa (Table 4).

4. Conclusions

The pressure drop in a fuel cell flow path is a key parameter for both performance and electrical efficiency of the system. In terms of the mass flow rate that flows into the porous layer, a higher pressure drop results, in most cases, in a greater value of ψ which is related to a greater amount of reactant available for the electrochemical reaction. Therefore, to the fuel cell designer and researcher concerning coherent flow-field design, fixing electrode characteristics such as the active area, backing permeability and GDL thickness etc.

References

1. A. Kazim, H.T. Liu and P. Forges, *J. Appl. Electrochem.* **29** (1999) 1409.
2. H. Dohle, R. Jung, N. Kimiaie, J. Mergel and M. Müller, *J. Power Sources* **124** (2003) 371.
3. G. Giacoppo, G. Squadrito, F. Urbani, E. Passalacqua and M. Badami (2003) 'Hydrogen power theoretical and engineering

solutions', Proceedings of HYPOTESIS V Porto Conte (Italy), 7–10 September 2003, pp. 707–716.
4. C.Y. Soong, W.M. Yan, C.Y. Tseng, H.C. Liu, F. Chen and H.S. Chu, *J. Power Sources* **143** (2005) 36.
5. S. Maharudrayya, S. Jayanti and A.P. Deshpande, *J. Power Sources* **138** (2004) 1.
6. G. Squadrito, O. Barbera, I. Gatto, G. Giacoppo, F. Urbani and E. Passalacqua, *J. Power Sources* **152** (2005) 67.
7. J.H. Ferziger and M. Perić, 'Computational Methods for Fluid Dynamics,' 3rd ed., (Springer, 2002).
8. D.P. Wilkinson and O. Vanderleeden *in* W. Vielstich, A. Lamm and H.A. Gasteiger (eds.), 'Handbook of Fuel Cells Fundamental Technology and Applications', Vol. 3 (Wiley, 2003), pp. 315–324.